High-throughput multispot single-molecule spectroscopy

Ryan A. Colyer[a*], Giuseppe Scalia[a], Taiho Kim[b], Ivan Rech[c], Daniele Resnati[c], Stefano Marangoni[c], Massimo Ghioni[c], Sergio Cova[c], Shimon Weiss[a], Xavier Michalet[a*]
[a]Department of Chemistry & Biochemistry, UCLA, Los Angeles, CA
[b]Nesher Technologies, Los Angeles, CA
[c]Dipartimento di Elettronica ed Informazione, Politecnico di Milano, Milano, Italy

ABSTRACT

Solution-based single-molecule spectroscopy and fluorescence correlation spectroscopy (FCS) are powerful techniques to access a variety of molecular properties such as size, brightness, conformation, and binding constants. However, this is limited to low concentrations, which results in long acquisition times in order to achieve good statistical accuracy. Data can be acquired more quickly by using parallelization. We present a new approach using a multispot excitation and detection geometry made possible by the combination of three powerful new technologies: (i) a liquid crystal spatial light modulator to produce multiple diffraction-limited excitation spots; (ii) a multipixel detector array matching the excitation pattern and (iii) a low-cost reconfigurable multichannel counting board. We demonstrate the capabilities of this technique by reporting FCS measurements of various calibrated samples as well as single-molecule burst measurements.

Keywords: single-molecule, photon counting, fluorescence, FCS, LCOS, CMOS, SPAD array, high-throughput.

1. INTRODUCTION

Fluorescence Correlation Spectroscopy (FCS) is a well-established single molecule technique for the observation of signal fluctuations due to molecular interactions or the diffusion of luminescent particles[1]. Since the signal fluctuations for diffusing particles are based on fluctuations in the number of molecules within a point-spread function (PSF), this constrains FCS to operating at low concentrations, which can result in long acquisition times. For purposes of rapid screening or the observation of diffusion parameters which change as a function of time, it is necessary to have a faster approach to the acquisition of FCS data.

By parallelizing FCS acquisition, we can obtain speed increases proportional to the degree of parallelization. Since several approaches to multi-pixel detectors have recently been developed and commercialized[2], this presents a new opportunity for high throughput FCS. However, high throughput FCS also requires a multi-spot excitation geometry, so that there is a unique point-spread function within the sample which can be mapped to each pixel of a multi-pixel detector.

There are a number of existing multi-spot generation methods, such as the use of microlens arrays with a static configuration [3], 2D fiber arrays (e.g., Silicon Lightwave Technology, Inc.), and the use of spatial frequency phase modulation with liquid crystal on silicon (LCOS) devices with computationally complex pattern generation[4, 5]. However, we desire an approach to multiple spot generation which is flexible, user-friendly, and rapidly adjustable so that the resulting excitation spots are mapped onto the target detector geometry.

We present a simple but relatively inflexible technique using a microlens array for multispot generation and contrast it with a new approach using a liquid crystal phase modulator to produce dynamically adjustable multiple PSFs, each of which is then mapped to a separate pixel of a multi-pixel CMOS SPAD detector. A further requirement for high throughput single-molecule spectroscopy is the simultaneous acquisition of data from multiple channels. We present an acquisition system using a custom programmed field programmable gate array (FPGA) with custom software to obtain

* ryancolyer@yahoo.com, michalet@chem.ucla.edu, Phone: 1-310-794-6693, Fax: 1-310-267-4672

Single Molecule Spectroscopy and Imaging III, edited by Jörg Enderlein, Zygmunt Karol Gryczynski, Rainer Erdmann,
Proc. of SPIE Vol. 7571, 75710G · © 2010 SPIE · CCC code: 1605-7422/10/$18 · doi: 10.1117/12.841398

data from many channels simultaneously.

Using this approach, both single molecule bursts and FCS data can be acquired in parallel from many points, allowing a much more rapid acquisition of low concentration diffusion information.

2. RESULTS

2.1 Microlens Array Point-Spread Function Measurements

We obtained 3D measurements of the excitation PSFs produced by our multi-spot microlens setup by using raster scanning of low concentration 100nm diameter fluorescent beads spin coated onto a coverslip. Figure 1 shows the results of this measurement, where each excitation spot can be seen to be close to the diffraction limit, and similar to a conventional single confocal excitation spot. Very faint "extra" spots can be seen on the fringes, which arise due to diffraction effects since the light for all of the spots is coherent. The z-extent of the PSFs is close to the theoretical expectation, except for the tendency toward a slight tilt angle toward the outermost spots, which is introduced by lens aberrations. This effect can be reduced by the selection of a larger diameter lens for the excitation path, but as it does not significantly alter the shape or volume of the peripheral PSFs, it has only a slight effect on our multi-spot measurements due to the overlap with the detection volume.

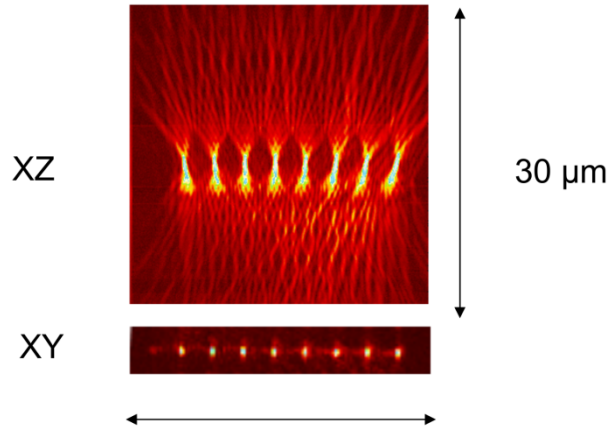

Figure 1. Scans in XZ and XY of a 100nm fluorescent bead showing the PSF cross-sections obtained with the microlens approach.

2.2 LCOS Point-Spread Function Analysis

Several significant difficulties exist in multi-spot microscopy, such as maintaining quality and uniformity of the PSFs for a large number of spots, and the simultaneous alignment of many spots. To address these difficulties, we developed a novel method for multi-spot generation with an LCOS[6]. To evaluate the experimental focal spot quality produced by this method, we used two different approaches. For the first approach we illuminated a bulk sample of Rhodamine 6G with the spot pattern and collected the emitted fluorescence using a CCD, as shown in Figure 2a. This shows the uniformity of the excitation spots, and the degree of uniformity of the illumination intensity. The slight decrease of intensity toward the periphery of the pattern is due to the intensity uniformity of the expanded beam incident on the LCOS.

For the second approach to measuring the excitation focal spots we used raster scanning of a 100nm fluorescent bead to examine the three-dimensional profile of the spots. An XZ cross-section of 8 spots is shown in Figure 2b. We have chosen a color pallet which shows the extended tails in the Z dimension so that one can observe the degree of PSF tilt introduced by spherical aberrations in the excitation path. This cross-section also shows that each excitation spot

occupies the desired femtoliter volume for single-molecule point measurements like FCS.

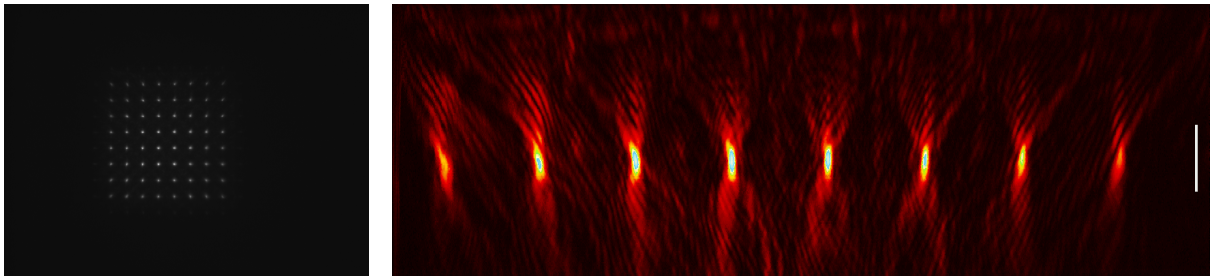

Figure 2. Measurements of the multiple PSFs produced by the LCOS excitation method, as measured by (a) a CCD measurement of Rhodamine 6G fluorescence, and (b) an XZ scan of a 100nm fluorescent bead (5um scalebar).

2.3 Detector Characterization

With the manufacture of single-pixel detectors it is feasible to choose the individual detectors with the best characteristics, while the rest can be discarded or used for low-demand applications. However with multiple pixel detectors this quickly becomes infeasible because each detector contains pixels with a distribution of the possible characteristics. Therefore it is necessary to characterize the individual characteristics of each pixel to ensure suitability for single-molecule experiments, and also so that these characteristics can be accounted for during analysis.

To accomplish this, we examined the dark counts and afterpulsing distribution for each pixel in our detector. The dark counts for each pixel (data not shown) were small in comparison to the FCS and burst count rates, and thus did not interfere significantly with the desired signal. We examined the afterpulsing distribution by performing an autocorrelation of the detector dark counts, as this low count rate is the condition in which afterpulsing is more clearly visible above the uncorrelated dark counts. As shown in Figure 3, we observe significant afterpulsing on a microsecond timescale, which follows a truncated power-law distribution. This distribution of afterpulsing is suitable for diffusion measurements with timescales of interest exceeding a few microseconds, as shown below.

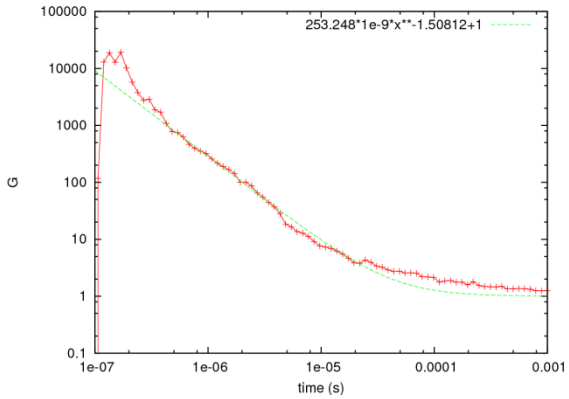

Figure 3. An autocorrelation function of one pixel's dark counts showing the temporal distribution of afterpulsing.

2.4 Burst Analysis

2.4.1 Fluorescent Beads

We obtained 10ms-binned time traces of sub-nanomolar concentrations of the free diffusion of 100nm fluorescent beads through the focal volumes created by the microlens setup. A representative time trace from a single channel is shown in Figure 4. While 68% of the total photon counts are due to the constant background, the rare burst events are clearly and

cleanly separated from this background, permitting easy burst analysis, and showing excellent suitability of the system for correlation analysis.

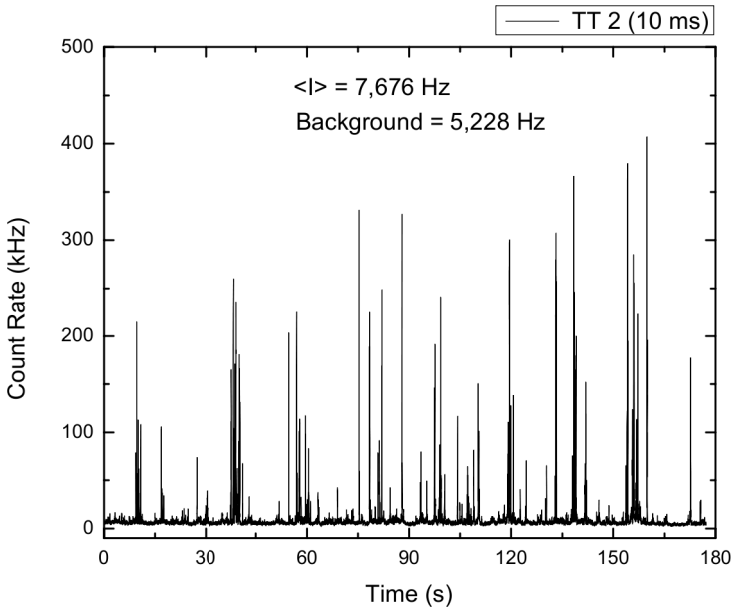

Figure 4. A representative portion of a time trace of fluorescent beads diffusing through one excitation PSF formed by the microlens setup, and acquired by one channel of the detector.

2.4.2 Cy3B-labeled DNA

To evaluate the system under more practical single-molecule conditions of the diffusion of single fluorophores, we performed a similar burst analysis using Cy3B-labeled single-stranded DNA, as shown in Figure 5. Clear bursts are discernible in the time trace, and the histogram of burst sizes shows a quasi-exponential distribution as expected theoretically[7].

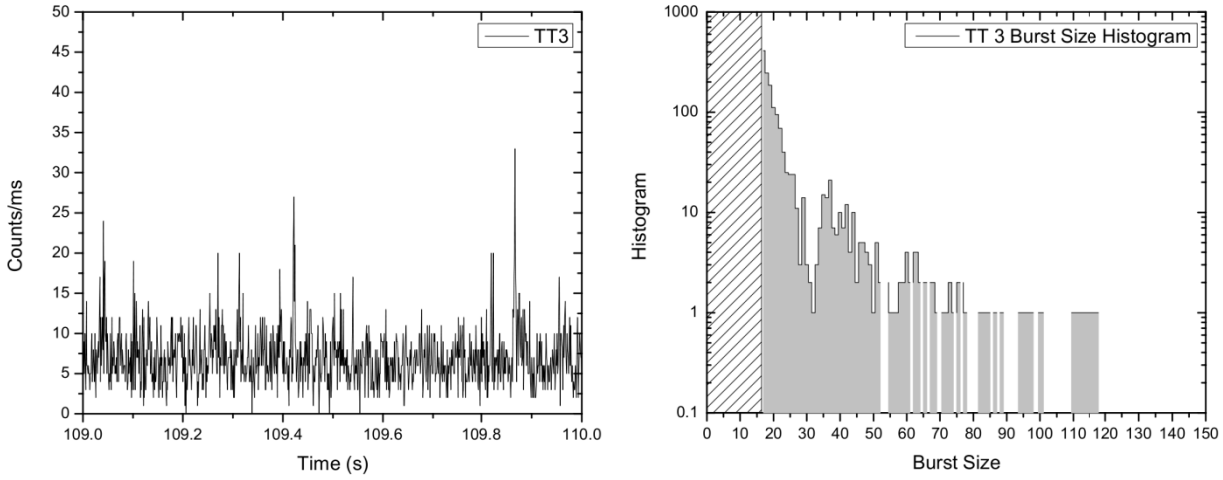

Figure 5. A (a) portion of a time trace and (b) burst size histogram for Cy3B-labeled single-stranded DNA.

2.5 Correlation Measurements

2.5.1 Fluorescent Bead Data

We acquired FCS data from multiple spots in parallel for a variety of bulk samples with nanomolar concentrations. To assess the linearity of our diffusion measurements we measured several samples of fluorescent spheres of known sizes, and compared the autocorrelation functions (ACFs) for each size and pixel.

Figure 6 shows the ACFs for 100nm bead data acquired with the microlens array setup using an 8x1 pixel geometry excited with a 488nm laser. A wide distribution of ACF amplitude values ($1/n$) values were observed with this configuration, but when the n values are normalized, as seen in Figure 6b, the ACFs have a high degree of overlap, indicating consistent diffusion time (d) values across the eight pixels, as shown in Table 1.

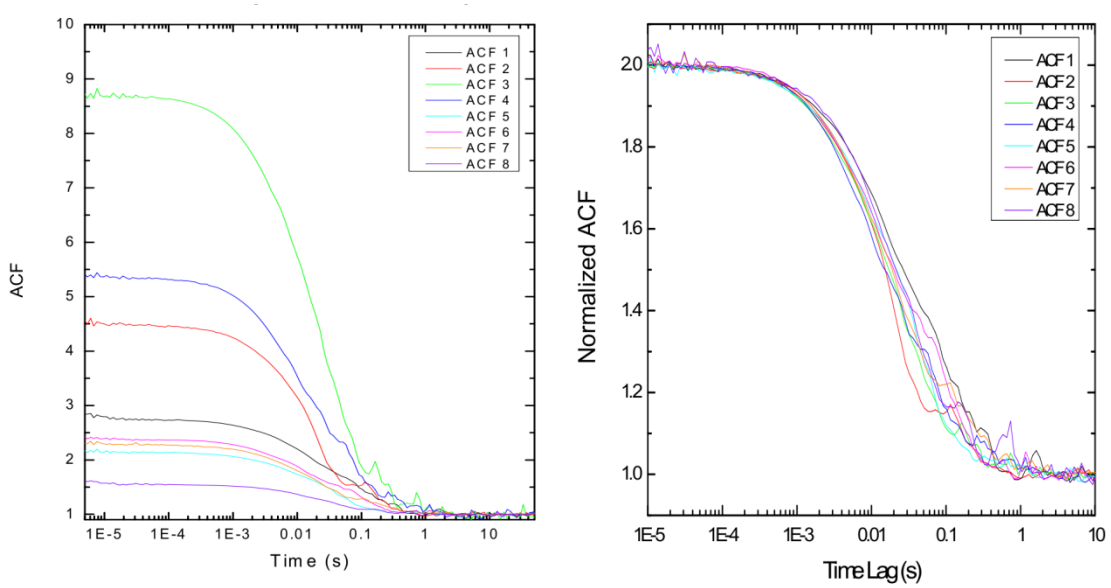

Figure 6. Autocorrelation functions for 100nm bead data acquired with microlens setup, plotted (a) showing the distribution of n values, and (b) normalized to the same n value.

#	1	2	3	4	5	6	7	8
n	0.58	0.29	0.13	0.23	0.88	0.74	0.79	1.83
d (ms)	28.5	13.9	16.1	16.3	19	21.4	19.1	21.2

Table 1. FCS fit parameters obtained across all 8 channels for 100nm diameter bead data on the microlens setup.

Two representative examples of single pixel ACFs for beads measured using the LCOS arrangement are shown in Figure 7, where fits were performed in the region above 50us to exclude the afterpulsing, which becomes dominant below 1µs. The two physically relevant parameters from the fit are n and d, as described in Equation 2, where n is proportional to the number of fluorophores in the focal volume, and d represents the typical time of diffusing through the focal volume.

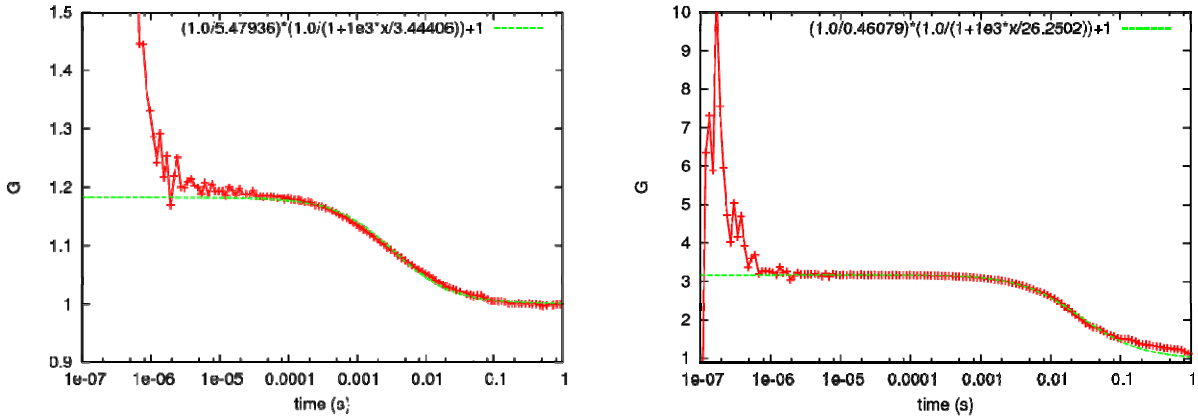

Figure 7. Two representative autocorrelation functions for 100nm bead data acquired with LCOS setup, acquired on two different channels.

Because the focal volume is highly elongated in the z-direction, in the ideal case only the width of the PSF in the XY plane significantly affects *d*, as well as the diffusion rate of the particles, which for free diffusion is primarily a function of hydrodynamic radius and viscosity. In practice, an imperfect PSF shape can introduce a slightly more complicated effect on *d* because of different XY widths at different points along z. The *n* parameter, however, can be significantly affected by the tails of the PSFs, since it is a function of the number fluctuations across the total PSF volume. Also, since multi-pixel detectors have a distribution of dark counts, pixels with significantly high dark counts relative to the signal count rate will result in a corresponding increase in the measured *n* value, which must be compensated for to extract the true number fluctuations.

With these effects in mind, we plot the distributions of *d* and *n* values as a function of channel number, as shown in Figure 8. In principle, the differences in channel width can be compensated for by independently calibrating the *d* values for each channel according to a known source, while the *n* values can be similarly calibrated using both a known source and a dark count measurement. This calibration procedure and its results will be detailed in a forthcoming publication.

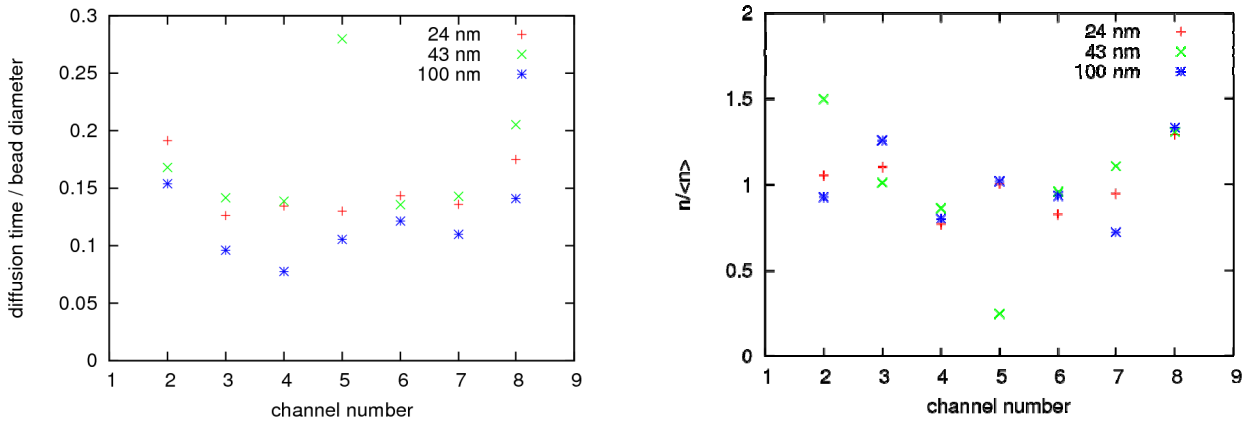

Figure 8. Plots of the (a) diffusion time and (b) average number of fluorophores in the focal volume, normalized such that they are independent of (a) bead size and (b) sample concentration. The 220nm bead sample has been omitted due to inadequate statistics, channel 1 is omitted due to hardware failure of that pixel, and the anomalous result for the 43nm beads in channel 5 is due to a single large aggregate which passed through that channel. The trends shown here from one channel to the next illustrate the parameters which can be used for calibration of the fit values.

To examine the linearity of the measured diffusion times, we performed experiments using various sizes of fluorescent beads. Figure 9 shows a plot of diffusion times (*d*) as a function of bead diameter. The expected relationship is

satisfactorily recovered. Slight deviations from linearity can be attributed to imperfections in the stability of the alignment.

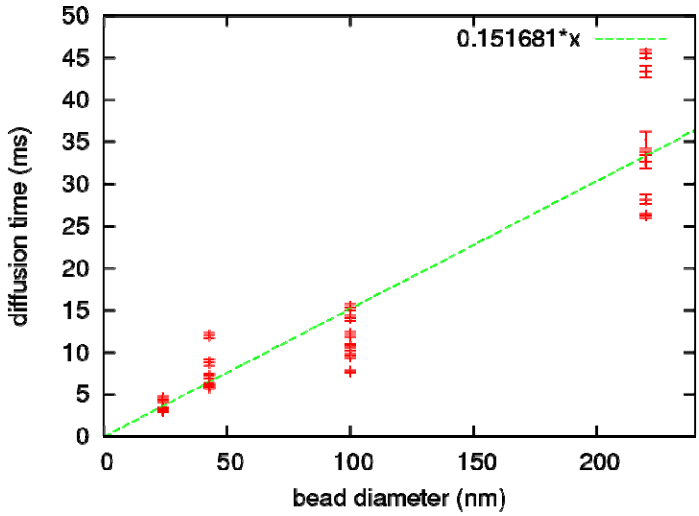

Figure 9. A linear fit to the diffusion times obtained for various sizes of fluorescent beads. The error bars are uncertainties of the fitted diffusion time.

2.5.2 Rhodamine 6G Data

To evaluate the capability of our system for performing single molecule measurements with single fluorophores, we performed a number of measurements of Rhodamine 6G (R6G) under various conditions. Two representative ACFs for R6G are shown in Figure 10. Because R6G diffuses much faster than fluorescent beads, the ACF has an inflection point which gets closer to the timescale of the afterpulsing. Therefore, to obtain a more accurate fit we include the afterpulsing function in our fits as shown. From these representative fits, it is apparent that the system is adequate for the observation of timescales down to 5µs.

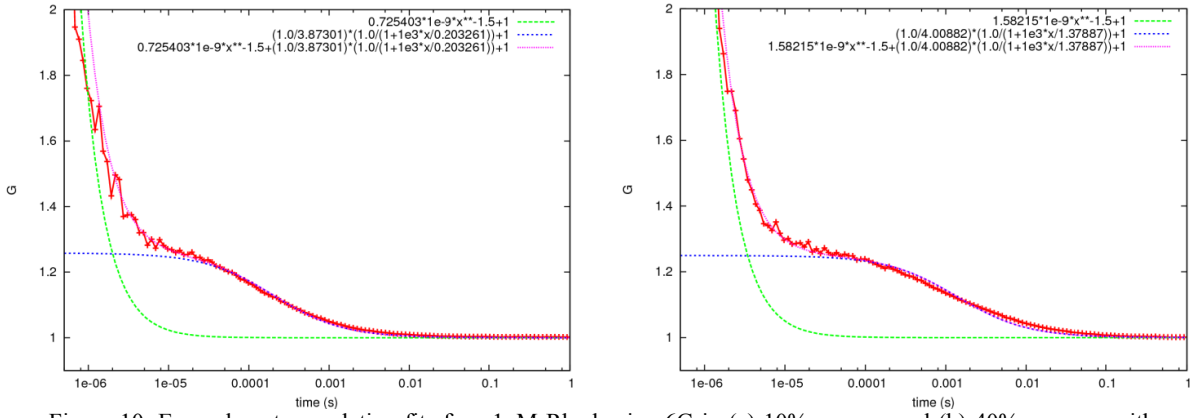

Figure 10. Example autocorrelation fits for ~1nM Rhodamine 6G in (a) 10% sucrose and (b) 40% sucrose, with detector afterpulsing included in the fits.

To examine the sensitivity of the system to varying diffusion rates for single-fluorophores, we prepared a viscosity series of R6G samples containing 10%, 20%, 30%, and 40% sucrose. The normalized ACFs for this series are shown in Figure 11a, where the increase in diffusion time with increasing viscosity is apparent. Figure 11b represents this same data with the diffusion time as a linear function of viscosity, where the expected relationship is observed. The width of the

distribution of diffusion times shown here is as explained above with the bead data, and can be similarly improved.

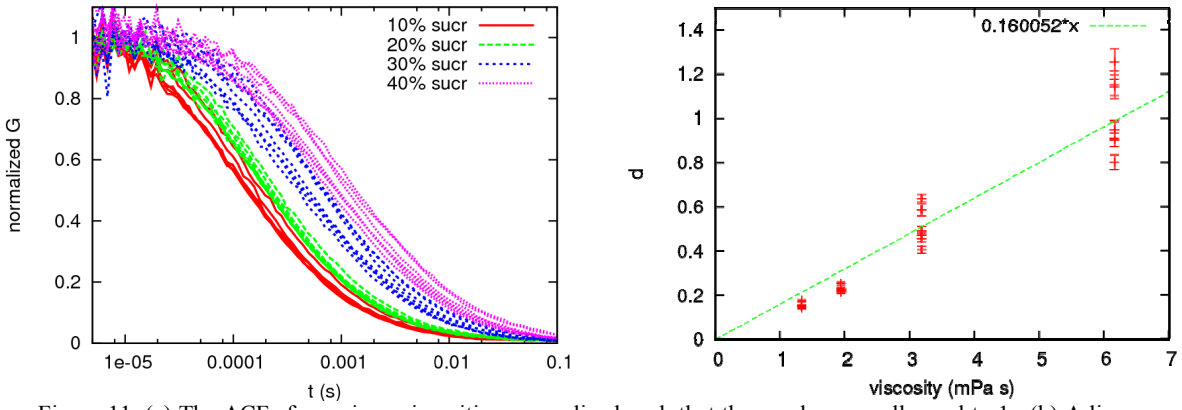

Figure 11. (a) The ACFs for various viscosities, normalized such that the n values are all equal to 1. (b) A linear fit to the diffusion times obtained with the various viscosity values. The error bars shown are from the uncertainty of the fitted diffusion times.

3. DISCUSSION AND CONCLUSIONS

We constructed a high-throughput system for single-molecule spectroscopy utilizing two different approaches to multi-spot excitation with multi-pixel detection. The microlens approach provided a low-cost approach with suitable PSF control and distribution for low to intermediate numbers of spots. The LCOS approach was more expensive, but provided a much more detailed and dynamic control over spot number, distribution, spacing, and orientation. This additional capability facilitated easy alignment and realignment, and also provided increased flexibility. This will enable the mapping of excitation spots to detectors with much larger numbers of pixels.

We demonstrated the capabilities of these systems for single-molecule spectroscopy using a variety of data such as single-molecule burst traces, burst size histograms, and analyses showing FCS curves with particle diffusion under various conditions. These demonstrations show that the systems are already capable of high-throughput single-molecule spectroscopy, which opens a variety of avenues for future work.

One straightforward approach to applying high-throughput processes to biologically relevant single-molecule spectroscopy would be to use these techniques with a multi-well setup. In such a setup, each excitation spot would be mapped to a single well of a multi-well chamber at the focal plane of the objective, and thus the multi-channel acquisition would correspond directly to a simultaneous multi-well acquisition. This would allow a single microscopy setup to simultaneously screen a large number of samples.

Another approach to applying our high-throughput system would be to acquire data for a single sample at a faster rate. This can be done by combining the data from each channel into a single measurement, resulting in the rate of data acquisition scaling linearly with the number of pixels. The decreased time for acquisition would provide a similar advantage to the multi-well approach, but it would also open up new opportunities for the observation of faster dynamics. Since most single-molecule measurements require the accumulation of large amounts of statistical information, a reduced time for acquiring this information means that changes in a sample's state can be compared at a shorter time, yielding the observation of faster dynamics.

The difficulties of an integrated high-throughput approach are primarily in the proper combination of data from non-equal channels. Steps to ensure the approximate equivalence of the excitation point-spread functions and alignment across all channels are important for easing this task, but for precision each channel will have to be calibrated so that integration can be done rigorously.

A further application of high-throughput single-molecule spectroscopy will be the rapid acquisition of Förster resonance energy transfer (FRET) data via two-color alternating-laser excitation (ALEX). Shorter acquisition times for low concentration FRET measurements would encourage a substantial increase in the usage of single-molecule FRET assays for diagnostic and drug-screening applications.

4. MATERIAL AND METHODS

4.1 Generation of multiple excitation spots with a microlens array

Performing confocal measurements with a multipixel detector requires the generation of multiple spots, and the most cost effective way to do this is to use a microlens array in the excitation path, as represented in Figure 12. A collimated beam entering the microlens array produces an array of focal spots at the focal distance of the lens, which can then be filtered by a spatial filter. We constructed a simple spatial filter out of a slit in a business card and two razor blades with a variable distance determined by a micrometer, allowing us one dimension with a fixed number of spots (8) and one dimension with a variable number of spots (1 or more). Then the focal spots are imaged by a recollimating lens, which passes the collimated light into the objective to form the spots at the focal plane of the objective. The emission light is then sent through a tube lens, which forms an image of the emission spots. Then a magnifying pair of lenses is used to adjust the pitch of the emission spots to match the precise pitch of the pixels in the multipixel detector.

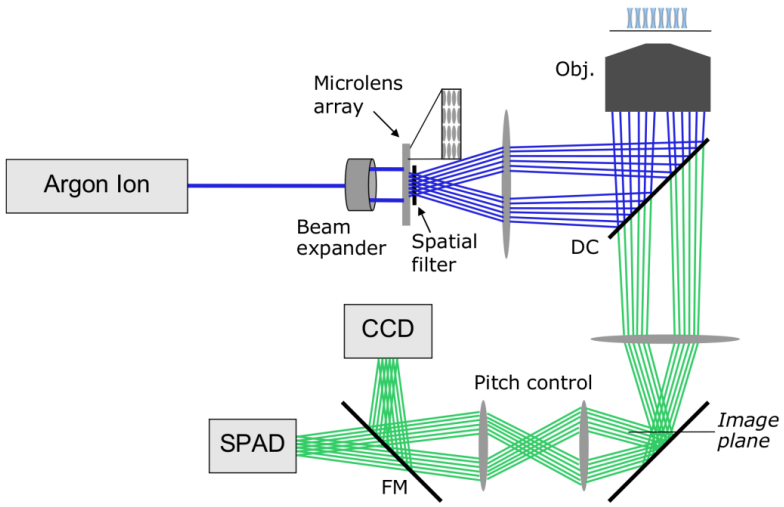

Figure 12. A schematic showing the experimental setup for the Microlens array approach.

4.2 Generation of multiple excitation spots with the LCOS

For more precise control over our multiple excitation spots, we also used a liquid crystal on silicon spatial light modulator (LCOS-SLM / LCOS) as a dynamically adjustable focal spot generator, which allows us to arbitrarily adjust the positions and spacing of the spots we generate. This approach allows us to rapidly generate new patterns using dynamically adjustable parameters, and allows us to easily resolve problems with zero-mode reflections from the LCOS. The technical details of the experimental setup and algorithm utilized will be presented in a forthcoming publication.

We also developed custom software using C and LabVIEW for the interactive generation of multi-spot patterns according to user-specified parameters. This software has a user interface permitting dynamic adjustment of the generated pattern of spots, allowing an interactive alignment process using the feedback from the detector channels to choose the optimal excitation arrangement. This was then used to generate multiple excitation spots at the focal plane of the objective which corresponded to multiple pixels at the detector plane.

4.3 Multi-pixel detection

For multi-pixel detection we used a custom detector consisting of eight single-photon avalanche photodiodes (SPADs) in a monolithic linear array, previously described by Rech et al. [8] This detector contains 8 SPADs which are each 50um in diameter, and spaced at a 250um pitch. The photon counting quantum efficiency is 50% at 550nm.

4.4 FPGA-based Multi-channel Data Acquisition

For multi-channel data acquisition we required a solution which was both efficient and scalable to large numbers of channels, so we developed a custom acquisition system using a Field Programmable Gate Array (FPGA) (PXI-7813R, National Instruments). Our custom FPGA firmware applies a time-stamp with 12.5ns resolution to each photon which arrives on each of the channels, and then combines this into a single data stream which allows the identification of which channel received a photon and what the time of arrival was.

Because we are scaling to large numbers of channels, while trying to preserve the full timing information, the total data throughput becomes a serious constraint. As a result, we constrain the data per photon count to a single 32 bit word to maintain a high throughput rate. Actual throughput has a complex dependence on system load, but we have obtained individual channel throughputs ranging from a few hundred thousand to a million counts per second.

4.5 Software

For control of the LCOS-generated excitation pattern we developed a custom pattern generation program using LabVIEW (National Instruments, Austin, TX) which allowed immediate adjustment of the number of spots in each dimension, the spacing of the spots, and the angular orientation of the pattern of spots. We also developed custom pattern analysis tools in C using the Huygens' Principle to simulate the excitation patterns which would be produced by a given LCOS pattern.

We then acquired the data from our customized FPGA setup using a custom acquisition program written in LabVIEW. It stores the raw data stream for later analysis, provides a visual representation of the intensity fluctuations in each channel, and plots time traces for selected channels during acquisition. The data file can then be subsequently loaded for burst analysis, or for autocorrelation[9, 10] as follows:

$$G(\tau) = \frac{\langle I(t)\rangle\langle I(t+\tau)\rangle}{\langle I(t)\rangle^2} \tag{1}$$

An additional custom LabVIEW program allows fitting of the resulting FCS curves according to the following formula:

$$G(\tau) = \frac{1}{n}\left(\frac{1}{1+\tau/d}\right) + 1 \tag{2}$$

For some fits a power law term was added to the fit equation to represent the afterpulsing. Some of the fits were performed with gnuplot, and scripted for batch processing of large numbers of files.

4.6 Samples

Rhodamine 6G was prepared in 1nM concentrations, calibrated using absorption spectrometry, and in a series of buffers containing 200mM NaCl combined with 0%, 10%, 20%, 30%, or 40% sucrose. Fluorescent beads (24nm diameter 535/575, 43nm diameter 580/605, 100nm diameter 540/560, 220nm diameter 535/575, FluoSpheres, Invitrogen, Eugene, OR) were prepared in sub-nanomolar concentrations by dilution in ultrapure water, followed by sonication and ultracentrifugation. The Cy3B measurements were acquired with Cy3B-labeled single-stranded DNA. The CCD

measurements of the PSFs were performed with micromolar concentrations of R6G, while the raster scanning PSFs were performed with low concentration 100nm fluorescent beads spin-coated onto a coverslip.

5. ACKNOWLEDGMENTS

This work was supported in part by NIH grants R01 GM084327 and R01 EB006353, and by NSF grant DBI-0552099. The work at Politecnico di Milano was supported in part by EC agreement 232359 (PARAFLUO) FP7-SME-2008-1. We thank Dr. Ted Laurence and Dr. Michael Culbertson for providing C code to implement multitau algorithms for time stamped and binned data, respectively.

REFERENCES

[1] Thompson, N.L., "Fluorescence Correlation Spectroscopy", in (Topics in Fluorescence Spectroscopy, Volume 1), J.R. Lakowicz, Plenum Press, New York, (1991).

[2] Ivan Rech, A.G., Franco Zappa, Massimo Ghioni, Sergio Cova, "High performance silicon single-photon avalanche diode array," Proc. of SPIE 7320(0H), 1-12 (2009).

[3] Hans J. Tiziani, H.-M.U., "Three-dimensional analysis by a microlens-array confocal arrangement," Applied Optics 33(4), 567-572 (1994).

[4] Bengtsson, J., "Design of fan-out kinoforms in the entire scalar diffraction regime with an optimal-rotation-angle method," Applied Optics 36(32), 8435-8444 (1997).

[5] Carsten Glasenapp, W.M., Holger Krause, Hans Zappe, "Biochip reader with dynamic holographic excitation and hyperspectral fluorescence detection," Journal of Biomedical Optics 12(1), 014038-1-8 (2007).

[6] Takashi Inoue, H.T., Norihiro Fukuchi, Munenori Takumi, Naoya Matsumoto, Tsutomu Hara, Narihiro Yoshida, Yasunori Igasak, "LCOS spatial light modulator controlled by 12-bit signals for optical phase-only modulation," Proc. of SPIE 6487(OY), 1-11 (2007).

[7] C. Eggeling, S.B., L. Brand, J.R. Fries, J. Schaffer, A. Volkmer, C.A.M. Seidel, "Data registration and selective single-molecule analysis using multi-parameter fluorescence detection," Journal of Biotechnology 86(163-180 (2001).

[8] I. Rech, D.R., S. Marangoni, M. Ghioni, S. Cova, "Compact-eight channel photon counting module with monolithic array detector," Proc. of SPIE 6771(13), 1-9 (2007).

[9] T.A. Laurence, S.F., T. Huser, "Fast, flexible algorithm for calculating photon correlations," Optics Letters 31(6), 829-831 (2006).

[10] M.J. Culbertson, D.L.B., "A distributed algorithm for multi-tau autocorrelation," Review of Scientific Instruments 78(4), 044102-1-6 (2007).